THE JOURNAL OF PHYSICAL CHEMISTRY B

Article

pubs.acs.org/JPCB

Host–Guest Interactions in Fe(III)-Trimesate MOF Nanoparticles Loaded with Doxorubicin

Resmi Anand,[†] Francesco Borghi,[§] Francesco Manoli,[†] Ilse Manet,[†] Valentina Agostoni,[‡] Pierluigi Reschiglian,[§,∥] Ruxandra Gref,*[,‡] and Sandra Monti*[,†]

[†]Istituto per la Sintesi Organica e la Fotoreattività, ISOF-CNR, Via Piero Gobetti 101, Bologna I-40129, Italy

[‡]Université Paris-Sud, UMR CNRS 8612, 5 rue JB Clément, Châtenay Malabry 92290, France

[§]Dipartimento di Chimica "G. Ciamician", Università di Bologna, Via Selmi 2, Bologna I-40126, Italy

[∥]byFlow Srl, Via Piero Gobetti 52/3, Bologna I-40129, Italy

Supporting Information

ABSTRACT: Doxorubicin (DOX) entrapment in porous Fe(III)–trimesate metal organic frameworks (MIL-100(Fe)) nanoparticles was investigated in neutral Tris buffer via UV–vis absorption, circular dichroism (CD), and fluorescence. The binding constants and the absolute spectra of the DOX-MIL-100(Fe) complexes were determined via absorption and fluorescence titrations. A binding model where DOX associates as monomer to the dehydrated Fe_3O $(OH)(H_2O)_2$ $[(C_6H_3)(CO_2)_3]_2$ structural unit in 1:1 stoichiometry, with apparent association constant of (1.1 to 1.8) × 10^4 M^{-1}, was found to reasonably fit the experimental data. Spectroscopic data indicate that DOX binding occurs via the formation of highly stable coordination bonds between one or both deprotonated hydroxyl groups of the aglycone moiety and coordinatively unsaturated Fe(III) centers. Complete quenching of the DOX fluorescence and remarkable thermal and photochemical stability were observed for DOX incorporated in the MIL-100(Fe) framework.

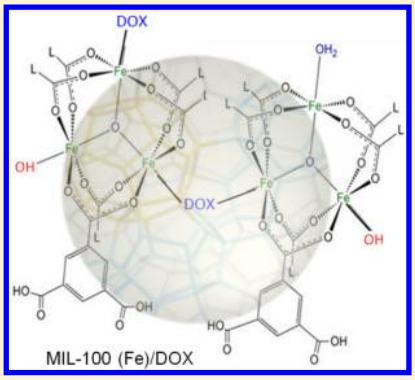

INTRODUCTION

The use of nanocarriers for drug delivery represents nowadays a promising approach to overcome a series of pharmacological shortcomings of drugs, like low target specificity, rapid clearance, poor pharmacokinetics, severe side effects, and multidrug resistance phenomena. To this purpose, a large variety of delivery systems has been investigated at both clinical and preclinical level, including polymeric nanoparticles, micelles, liposomes, and various metal-based nanoassemblies.[1−3] In this frame, delivery of anticancer drugs received particular attention due to the existence of severe side effects.[4,5] Liposome-based formulations of doxorubicin (DOX), coated (Doxil and Caelyx)[6,7] or not (Myocet)[8] with poly(ethylene glycol), and albumin nanoparticles containing paclitaxel (Abraxane)[9] have been successfully introduced in the clinical practice, and several other nanocarrier–anticancer drug formulations are presently under clinical trials. A significant added value can come from nanoparticles able to accomplish multimodal or theranostic functions by incorporating multiple drugs, targeting ligands, and imaging agents.[10]

A recent innovative class of multifunctional nanoparticles is based on metal organic frameworks (MOFs). MOFs are hybrid crystals composed of metal ions or clusters connected by multidentate organic ligands to form one-, two-, or three-dimensional metal–organic arrays possessing a structure with very high porosity and enormous surface area. MOFs are highly tunable in terms of chemical composition, eventually determining their crystal structure, the dimensions of the pores, as well as their physicochemical properties.[11,12] Because of their unique features, they are used in a large variety of scientific and technological areas, mainly relevant to catalysis, separation, gas storage, sensing, magnetic, and electrooptical materials. More recently, MOFs have attracted increasing interest for biomedical applications.[13−21] For a very recent collection of comprehensive reviews, we refer to the 2012 special issue of *Chemical Reviews* on Metal Organic Frameworks.[22]

Because of their amphiphilic character and the presence of accessible Lewis acidic metal sites or functional groups, nanoscale MOFs efficiently encapsulate various challenging therapeutic molecules, among which are anticancer drugs such as busulfan[23] and doxorubicin (DOX).[24] In addition to the high loading, controlled release in simulated body fluid could be achieved. Moreover, Fe(III) nanoMOFs exhibit interesting magnetic resonance imaging properties useful for theranostics.[24] A family of biodegradable MOFs, based on Fe(III) clusters and polycarboxylate ligands, has been synthesized[25,26] and recently transposed under the nanoscale regime following "green" technology.[27−29] Such materials proved to act as efficient "molecular sponges", rapidly soaking important

Received: April 18, 2014
Revised: May 30, 2014
Published: June 24, 2014

   dx.doi.org/10.1021/jp503809w | J. Phys. Chem. B 2014, 118, 8532–8539

amounts of hydrophilic and hydrophobic drugs directly from aqueous solutions.[24] As previously mentioned, DOX (Scheme 1) is one of the drugs successfully incorporated in MIL-100

Scheme 1. Doxorubicin (Adriamycin) Molecular Structure

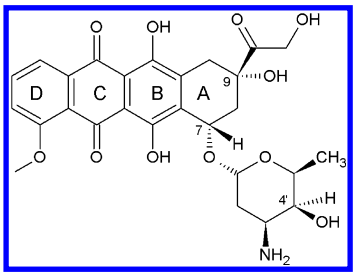

(Fe) (MIL standing for Material of Institut Lavoisier), one of the most promising among the nanoMOF materials. MIL-100 (Fe) is made of trimers of Fe(III) octahedra linked by benzene-1,3,5-carboxylate units in a framework characterized by mesoporous cages with rigid structure. DOX loadings reached ca. 9 wt %, and the drug was slowly released over several days.[24] DOX is the prototypical antitumoral drug of the anthracycline family, suited for the treatment of leukemia and various solid tumors.[30] Because of its great efficacy, it is still widely employed despite severe side effects mainly related to cardiotoxicity.[31] The cardiotoxicity of anthracyclines has been related to their redox activity and thought to be controllable by delivering the drugs as Fe(III) complexes.[32] Other shortcomings of DOX are its self-association tendency in aqueous solution, affecting both cellular uptake and biological activity[33,34] and the appearance of cancer cell drug resistance.[35] The search for new nanosized carriers for DOX, able to contrast such drawbacks, is attracting much attention.[36−40] In this frame, the incorporation of DOX in the MIL-100 (Fe) nanoscale MOFs holds an interesting potential.[24]

We provide a characterization of the MIL-100(Fe)-DOX complexes in aqueous medium using UV−vis absorption, circular dichroism (CD), fluorescence, and dynamic light scattering (DLS). The thermal and photochemical stability of the complexes was also checked to get information on the possible occurrence of iron-induced free-radical chemistry in the system.

EXPERIMENTAL SECTION

Materials. Doxorubicin (DOX, Adriamycin, Scheme 1), from ALEXIS Biochemicals, was used as received. Water was purified by passage through a Millipore Milli-Q system. 0.01 M Tris buffer at pH 7.4 was used. MIL-100 (Fe) nanoMOFs were synthesized by a hydrothermal microwave-assisted reaction and characterized as previously described.[27] In brief, a mixture of Fe(III) chloride hexahydrate (6.0 mmol; Alfa Aesar, 98%) and 1,3,5-benzenetricarboxylic acid (4.02 mmol; trimesic acid or 1,3,5-BTC, Aldrich, 95%) in 20 mL of deionized water was heated 6 min at 130 °C under stirring. The power applied was 400 W (Mars-5, CEM, U.S.: power maximum output 1600 W, frequency at full power 2450 MHz). The nanoMOFs were recovered by centrifugation 10 min at 10 000*g* and washed six times with absolute ethanol to remove the residual non reacted organic acid. The crystallinity of MIL-100 nanoMOFs was assessed by X-ray powder diffraction (XRPD). X-ray patterns were collected in a conventional high-resolution (θ-2θ) D5000 Bruker diffractometer (λ_{Cu} Kα,Kα_2) from 3 to 20° (2θ) using a step size of 0.02 and 4° per step in continuous mode. (See Figure S1 in the SI.)

The nanoparticle size and morphology were characterized by DLS (Malvern Nano-ZS, Zetasizer Nanoseries, U.K.), and transmission electron microscopy (TEM; Darwin; 208 Philips; 60−80−100 kV; Camera AMT) showed typical faceted structures. (See Figure S1 in the SI.) Surface morphology of gold-coated samples was investigated with a field-emission scanning electron microscope (FESEM, Gemini Columns SIGMA Zeiss, DE) operating at 1.5 keV, at a working distance of 3 mm, and the images with the in-lens secondary electron detector were collected . (See Figure S1 in the SI.)

The porous surface was measured by nitrogen sorption experiments at −196 °C on a ASAP 2020 (Micromeritics) after sample's outgassing at 150 °C for 18 h under secondary vacuum. The calculated Langmuir surface was 1350 ± 100 m^2 g^{-1}.

The crystalline material is made of oxocentered trimers of Fe(III) octahedra linked by benzene-1,3,5-tricarboxylate ligands (1,3,5 BTC), resulting in hybrid supertetrahedra, which further assemble in nanoMOFs with a zeolitic-like architecture (Scheme 2). This frame delimits very large pores (free

Scheme 2. Coordination between Fe(III) Trimers and Benzene-1,3,5-tricarboxylic Acid (Trimesic Acid) (1,3,5 BTC) Leads to the Formation of Hybrid Supertetrahedra That Further Assemble into a Zeolitic-Like Architecture (See Text) under the Form of Submicronic Nanoconstructs (nanoMOFs)[25,26]

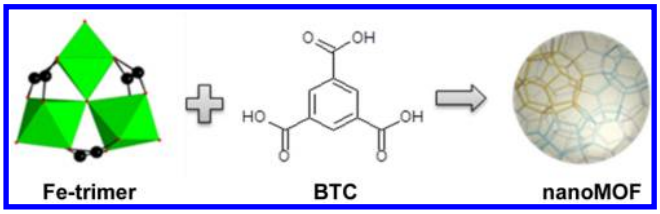

diameters of 25 and 29 Å) accessible through pentagonal and hexagonal microporous windows (of ca. 5.5 and 8.6 Å).[25,26] Fe(III) trimers in MIL-100 possess accessible coordinatively unsaturated metal sites (CUS), up to two per trimer, able to coordinate a wide range of polar species and drugs.[41] Molar absorption coefficients and binding constants in the present work are referred to the trimeric Fe(III) unit of MIL-100 (Fe) with structural formula Fe_3O $(OH)(H_2O)_2$ $[(C_6H_3)(CO_2)_3]_2$ (dehydrated form).

Sample Preparation. MIL-100 (Fe) nanoMOFs were stored in the dark at room temperature as EtOH wet material or ethanolic concentrated suspension. An aliquot was dispersed in a few milliliters of ethanol. The suspension was first centrifuged (10 min, 8000 g). Next, the sedimented nanoMOFs were separated from the supernatant, washed extensively, and resuspended either in tris(hydroxymethyl)aminomethane (Tris) buffer (10^{-2} M, pH 7.4) or in pure water. NanoMOFs final suspensions and mixtures with DOX were gently stirred for at least 30 min at room temperature and kept under stirring during the time span of the experiments. SEM shows that the organization of MIL(100) Fe in small particles is maintained after DOX loading. (See Figure S2 in the SI.) Tris buffer, used to improve the drug solubility and optimize the spectroscopic study (see also the investigation of the binding of phosphorylated AZT derivatives to the nanoMOFs),[27]

dx.doi.org/10.1021/jp503809w | J. Phys. Chem. B 2014, 118, 8532−8539

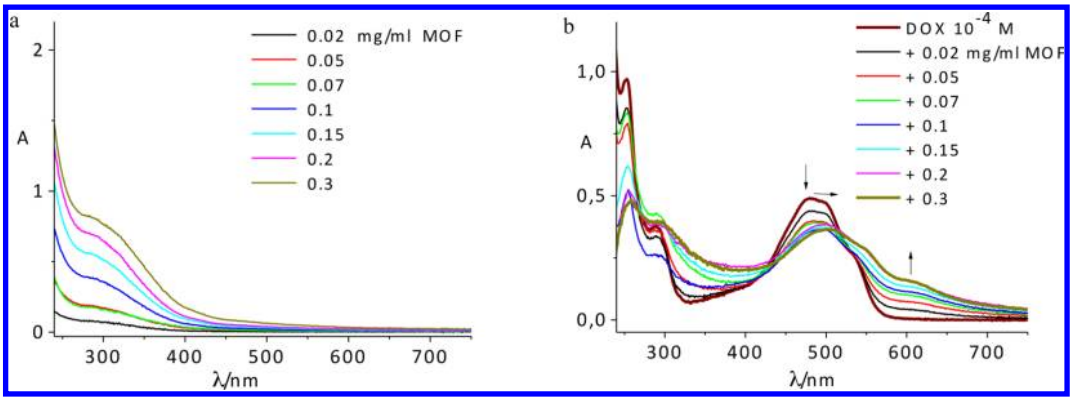

Figure 1. Absorption spectra of MIL-100 (Fe) nanoparticle suspensions with material content from 0.02 to 0.3 mg/mL (a) in neutral Tris buffer and (b) in the presence of DOX 1×10^{-4} M. In the latter case, MIL-100 MOF suspensions in Tris buffer were used as reference. Cell path length 0.5 cm, T = 22 °C.

promotes the formation of somewhat larger particles compared with pure water. (See DLS data below.)

Binding Constants. To estimate the apparent binding constant (K_a) of DOX to the MOF frame, DOX–MOF mixtures (DOX 1×10^{-4} M and various MOF contents in Tris buffer) were centrifuged for 20 min at 8000 g. All MOFs settled down, whereas free DOX remained in the supernatant and was quantified by UV–vis absorption using a molar absorption coefficient of 10 800 $M^{-1}cm^{-1}$ at 480 nm.[42] We expressed the total host concentration x in terms of the concentration of the dehydrated $Fe_3O(OH)(H_2O)_2[C_6H_3(CO_2)_3]_2$ MOF structural unit (named "Fe(III) trimer" in the following) and for the sake of simplicity assumed the formation of a DOX–Fe(III) trimer complex with a 1:1 stoichiometry. From the definition of the dissociation constant K_d (= $1/K_a$), eq 1 relates the bound DOX concentration to the total host concentration x

$$[\text{bound DOX}] = 1/2(K_d + x + c - ((K_d + x + c)^2 - 4xc)^{1/2}) \quad (1)$$

where c is the total DOX concentration.

Spectroscopic Measurements. UV–vis absorption spectra were recorded with a PerkinElmer λ9 spectrophotometer equipped with an integrating sphere to avoid distortion of the absorption profiles due to light scattering by the nanoMOFs. All measurements were carried out at 22 °C in 0.2 or 0.5 cm path length quartz cuvette using Tris buffer or the relevant MOF-alone suspension as the reference. CD spectra were taken on a Jasco J-715 spectropolarimeter. The signal of the cell filled with the nanoMOF suspensions was subtracted. Fluorescence spectra of air-equilibrated solutions were registered on a SPEX Fluorolog 111 spectrofluorimeter. Fluorescence lifetimes in air-saturated solutions were measured with a time-correlated single-photon counting system (IBH Consultants). A nanosecond LED at 465 nm was used as the excitation source, and the emission was detected at 590 nm. The software package for analysis of emission decays was provided by IBH Consultants.

Nanosecond Laser Flash Photolysis. The setup, based on a Nd:YAG laser (20 ns fwhm, 2 Hz) as excitation source and a pulsed high pressure Xe arc as analyzing light in right-angle geometry, was already described.[42] Laser pulses of 4 to 5 mJ at 532 nm were used.

RESULTS AND DISCUSSION

UV–vis Absorption. The absorption spectra of the MIL-100 (Fe) MOF suspensions at various concentrations in Tris buffer 0.01 M at pH 7.4 are shown in Figure 1a. The Fe-trimesate coordination band appears in the 300–400 nm region. An apparent molar absorption coefficient of 2900 M^{-1} cm^{-1} was calculated at 330 nm from the linear dependence of the absorbance on the Fe(III) trimer content (MW 653). This value is in agreement with reported absorption coefficients of Fe-carboxylate LMCT absorption bands.[43] Figure 1b shows the absorption changes observed in a solution of DOX 1×10^{-4} M in Tris buffer upon titration with the MOFs. On increasing the MOF content, the absorbance increases in the 300–430 nm region and decreases at 430–520 nm, while the absorption band shifts to the red and a structure arises in the 520–750 nm region.

To properly interpret these spectral changes, it is worth recalling that the absorption spectrum of DOX displays bands at 288 and 480–500 nm, relevant to the two allowed $^1A \rightarrow {}^1L_a$ and $^1A \rightarrow {}^1L_b$ π,π^* transitions polarized along the short and long axis of the dihydroxyanthraquinone moiety, respectively. The shoulder around 320–380 nm is associated with n,π^* transitions of the three C=O groups in the molecule, weakly allowed by electric dipole. At neutral pH, the aglycone part is neutral, whereas the daunosamine moiety is protonated.[44,45] Deprotonation of the phenolic OH groups of the aglycone ring B upon pH increase (pK values of 10.16 for C_{11}–OH and 13.2 for C_6–OH) produces spectral modifications quite similar to those of Figure 1b.[42,46] This finding suggests that DOX incorporation into the MOF frame is mediated by deprotonation of hydroxyl groups of the aglycone moiety, most likely involved in coordination to Fe(III) centers. Further support for this conclusion comes from the similarity of the UV–vis absorption spectra of DOX-MOF mixtures to those of DOX solutions with free Fe(III) ions, in which up to three drug molecules are coordinated with release of one proton per bound unit.[32,47] Various binding modes of DOX to Fe(III) ions have been suggested: bidentate chelation at the quinone-hydroquinone sites of the C–B rings,[32,47,48] coordination to the C14 hydroxyl group of the α-ketol side chain,[49−52] and formation of a cage-like structure involving the two quinone oxygens, an α-hydroxy terminal group, and the ketone of the C9 side group.[53] Interactions of Fe^{3+} with daunosamine moiety and the C4 methoxy group have also been indicated to promote the anthracycline-iron complexation.[54,55] Close inspection of

dx.doi.org/10.1021/jp503809w | J. Phys. Chem. B 2014, 118, 8532–8539

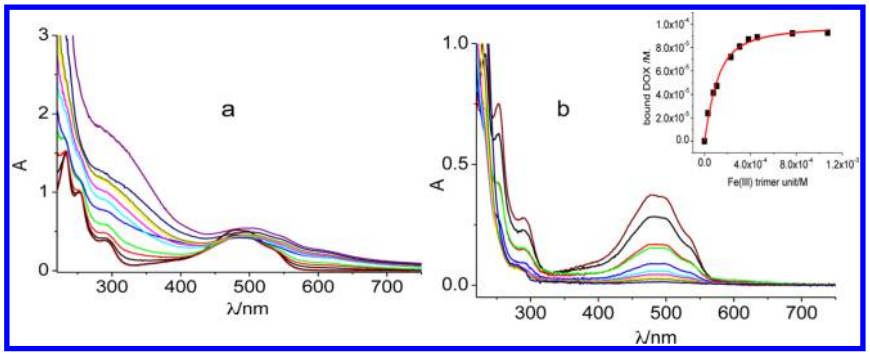

Figure 2. Absorption spectra of DOX 1×10^{-4} M in the presence of MIL-100 (Fe) from 0 to 0.7 mg/mL in neutral Tris buffer. (a) Suspensions before centrifugation; (b) supernatant after centrifugation. Cell path length 0.5 cm, pure Tris buffer as reference, T = 22 °C.

the spectra in Figure 1b reveals the presence of quasi-isosbestic points at 420 and 530−540 nm for MOF content ≤0.1 mg/mL, which are lost at higher MOF contents. This fact points to the existence of more than one type of DOX-Fe(III) complex in the MIL-100(Fe) nanoparticle frame.

The average association constant of DOX was estimated by titrating a solution of DOX (1×10^{-4} M) with MOFs up to the Fe(III) trimer unit concentration of 1.1×10^{-3} M (MOF content ≤0.7 mg/mL). Centrifugation of the DOX−MOF mixtures (Figure 2a) and quantification of the free DOX in the supernatant was performed using a molar absorption coefficient of 10 800 M^{-1} cm^{-1} at 480 nm. (See Figure 2b.) From the plot in the inset, a value $K_a = (1.8 \pm 0.1) \times 10^4$ M^{-1} was extracted by applying eq 1. The good quality of the best fit and the small error indicate that the 1:1 stoichiometry model (one DOX molecule bound on average to one Fe(III) trimer) fairly well applies under the conditions of the experiment. The apparent association constant is by six to seven orders of magnitude lower than those reported for DOX binding to free Fe(III) ions.[47] This is rationalized considering that DOX binding can occur both inside the MOF frame and on the nanoparticle outer surface. A reduced accessibility of the Fe(III) CUS sites inside the MOF pores can be justified by the small size of the pore windows.

Circular Dichroism. DOX has several asymmetric carbon centers. The C7 and C9 configurations are of particular importance for the chirality in the UV−vis region (Scheme 1).[44,45] The CD spectrum of a DOX 1.0×10^{-4} M solution in neutral Tris buffer is characterized by negative bands at ca. 290 and 500−550 nm and positive bands at ca. 250, 350, and 450 nm. A positive−negative splitting of the dichroic signal in the 400−600 nm region is due to the presence of DOX in dimeric form. The negative component is weaker than the positive one and is barely observable under the present conditions, despite the fact that dimeric DOX is predominant. (DOX monomer is only 23%, according to log (K_{dim}/M^{-1}) = 4.84 in neutral aqueous buffer.)[42] The formation of the DOX-MOF complexes deeply modifies the CD spectral profiles (Figure 3). The changes depend on the MOF content of the solutions: on adding increasing amounts of MIL-100 (Fe) material from 0 to 1 mg/mL (corresponding to 1.5×10^{-3} M trimer unit concentration), the signal at 250 nm first increases then decreases, the bands at 290 (negative) and at 350 nm (positive) slightly increase then progressively decrease in intensity, and the positive band at 450 nm first increases then disappears; a positive band raises at ca. 500 then decreases; the negative signal at 500−550 nm becomes positive and new bands appear in the red region, with λ_{max} progressively shifting from ∼600 nm at 0.01 mg/mL to ∼650 nm at 1 mg/mL MOF content. The disappearance of the negative signal at 500−550 nm indicates that complexation is accompanied by monomerization of DOX. This result is somehow expected because the DOX dimer is likely too large to pass across the 5.5 or 8.6 Å wide windows of the pores. The shift of the CD signal to longer wavelengths is qualitatively similar to that observed in neutral DOX solutions on the addition of free Fe(III) ions with increasing metal-to-ligand molar ratios and is attributed to coordination of one metal ion at C(11)-O^- ($\lambda_{max} \cong 600$ nm) or two metal ions at C(11)-O^- and C(6)-O^- ($\lambda_{max} \cong 650$ nm).[48] Thus, CD clearly indicates that DOX coordination in nanoMOFs can involve one or two Fe (III) centers, depending on the MOF content. Binding modes such as those represented in Scheme 3 can be hypothesized, where up to two monomeric drug molecules access CUS of Fe(III) atoms and establish monodentate bonds, replacing previously coordinated water molecules. In the schematic representation, the crystal network is maintained, but the actual crystallinity of the drug-loaded particles has not been investigated. Two spatially close Fe centers could, in principle, be connected by one DOX molecule. The formation of DOX bridges only at high MOF contents suggests that this binding mode can be associated with particle aggregation. Confirmation of this assumption comes from DLS measurements.

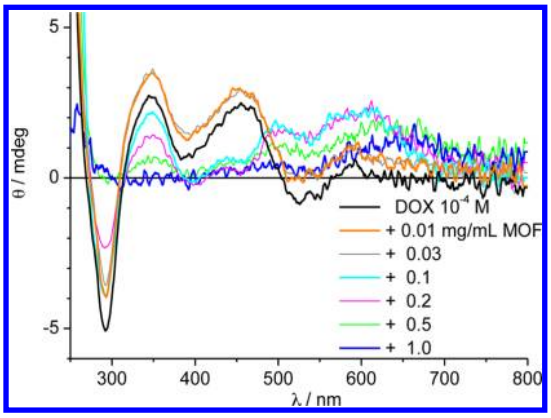

Figure 3. Ellipticity of DOX 1×10^{-4} M in neutral Tris buffer in the absence and in the presence of MIL-100 (Fe) nanoparticles with concentrations ranging from 0.01 to 1 mg/mL, with subtraction of MOF signal. Cell path length 0.5 cm, T = 22 °C. CD profiles were smoothed.

Dynamic Light Scattering. We performed DLS experiments on freshly prepared suspensions of MIL-100 (Fe) with MOF content between 0.02 and 0.7 mg/mL both in 10^{-2} M

dx.doi.org/10.1021/jp503809w | J. Phys. Chem. B 2014, 118, 8532−8539

Scheme 3. Schematic Representation of the MIL-100 (Fe) Structure and the DOX Interaction[a]

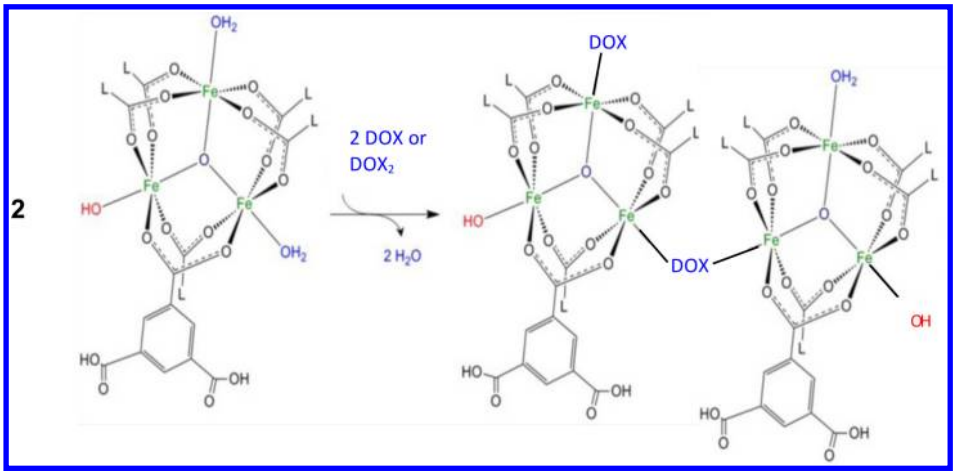

[a]Up to two DOX molecules may interact with each Fe(III) trimeric unit by coordination to CUS of Fe(III) centers, replacing previously coordinated water molecules. One or two coordination bonds per DOX monomer can be formed.

Tris buffer of pH 7.4 and in pure water in the absence and presence of 1×10^{-4} M DOX. All the measurements were carried out within 90 min from sample preparation. Polydispersity indexes were in the range 0.15 ± 0.05. The results are collected in Table 1. In the absence of DOX, the particle size is independent of the MOF content but depends on the medium: the mean hydrodynamic diameter ranges from 450 to 700 nm in Tris buffer, whereas it is about 200−250 nm in water. In both media, an increase in the mean hydrodynamic diameter (up to >1500 nm) with increasing MOF content was observed in the presence of DOX, reasonably reflecting drug-induced nanoparticle aggregation. (See also the DLS experiment reported in Table S1 in the SI.) DLS data are thus consistent with UV−vis absorption and CD data, suggesting a coordination mode of DOX where drug molecules bound on the surface of the MOFs act as linkers between Fe centers of different nanoparticles via the dihydroxyanthraquinone moiety.

Table 1. Average Values of Hydrodynamic Diameter (Φ) Measured by DLS in Freshly Prepared Samples of MIL-100 (Fe) in the Absence and Presence of DOX 1×10^{-4} M in 10^{-2} M Tris buffer pH 7.4 and in Water, T = 25 °C

MOF (mg/mL)	Φ MOF in Tris (nm)[a]	Φ MOF + DOX 1×10^{-4} M, in Tris (nm)[a]	Φ MOF in water (nm)[a]	Φ MOF + DOX 1×10^{-4} M in water (nm)[a]
0.02	452	520	256	215
0.05	646	500		209
0.1	458	538	215	208
0.2	698	854		
0.5	596	932		
0.7	592	1558	238	1667

[a]Uncertainty is within 10%.

In view of the application of MIL-100 (Fe) in drug-delivery devices, nanoparticle aggregation should be avoided as much as possible.[56−58] In the case of DOX 10^{-4} M in water, this requisite could be safely achieved maintaining the MOF content below 0.2 mg/mL (Table 1). Under such conditions the nanoparticle diameter measured by DLS does not appear to be markedly modified upon drug loading. Size distribution broadens more at higher MOF contents. (Figure S3 in the SI.)[24,27,59,60] Concerning the fate of the MOFs in a

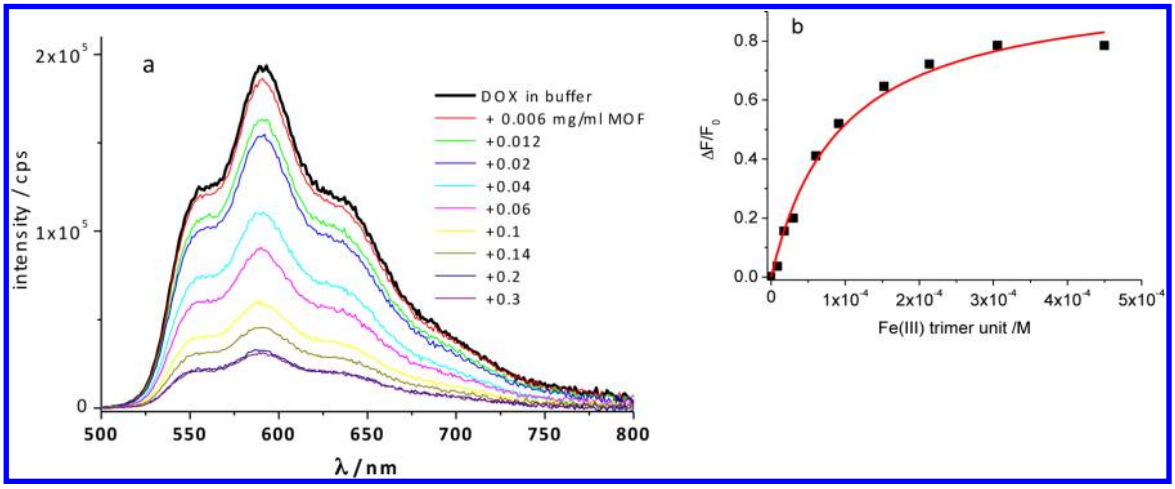

Figure 4. (a) Fluorescence spectra of DOX 2×10^{-5} M in the absence and presence of MIL-100 (Fe) from 0.006 to 0.3 mg/mL in neutral Tris buffer. Excitation at 480 nm, T = 22 °C. (b) Fraction of emission intensity lost at 590 nm, corrected for the absorbance changes at 480 nm along with the titration (■) and best fit to eq 2 (red solid line).

dx.doi.org/10.1021/jp503809w | J. Phys. Chem. B 2014, 118, 8532−8539

physiological environment, they will be further diluted in the bloodstream after intravenous administration. Moreover, they will get in contact with the multitude of plasma proteins that tend to adsorb drugs at their surface and will compete for DOX binding. It has been previously shown that in the presence of plasma, the MIL-100 (Fe) nanoMOFs are stable and that phosphate salts tend to coordinate to the MOF frame favoring release of DOX from the pores.[24]

Fluorescence. The binding of DOX to nanoMOFs was also monitored by means of fluorescence. A 2.0×10^{-5} M DOX solution in neutral Tris buffer exhibits a structured fluorescence spectrum with λ_{max} = 590 nm (Figure 4). The decay of the emission in the nanosecond time domain is monoexponential with τ_1 = 1.0 ns (χ^2 = 1.02) and is dominated by the DOX monomer.[40,42,61] The addition of increasing amounts of MOFs determines a progressive decrease in the emission intensity with no change in the spectral shape. The decay kinetics remains monoexponential with unchanged lifetime, unequivocally indicating the occurrence of static quenching due to the formation of non emissive ground-state complexes. (See Figure S4 in the SI.) These findings are consistent with existing knowledge on the nonfluorescent nature of Fe(III)−DOX complexes, where DOX is present in the basic form, and further support that binding to the MOF frame is accompanied by deprotonation of the dihydroxyanthraquinone moiety. DOX fluorescence quenching in the MOFs might, in principle, involve (i) an efficient nonradiative deactivation of the excited state by internal conversion or intersystem crossing to the triplet manifold or (ii) an electron transfer with the formation of free radicals. Nanosecond laser flash photolysis at λ_{exc} = 532 nm did not reveal any transient (triplet or radical) in the MIL-100 (Fe)−DOX system. Thus, either formation of an intrinsically nonfluorescent excited state or an electron transfer to the excited molecule, followed by charge recombination on the subnanosecond time scale, may be at the basis of the quenching of the DOX emission within the MOFs.

The changes in the DOX fluorescence intensity upon titration with the MOFs can be used to determine the apparent association constant K_a for 1:1 complex formation, applying the theory of static quenching. The fraction of bound DOX is expressed in terms of the amount of lost fluorescence, according to eq 2

$$\Delta F/F_0 = K_a x/(1 + K_a x) \quad (2)$$

where F_0 is the total fluorescence intensity of DOX in neutral buffer, ΔF is the emission intensity lost in the presence of the MOFs, and x is the concentration of the Fe(III) trimers, in excess over DOX under most of the titration conditions.[62] From the plot of Figure 4b, a value $K_a = (1.1 \pm 0.1) \times 10^4$ M^{-1} was extracted, in fairly good agreement with the K_a value extracted from data in Figure 2, considering that UV−vis absorption and fluorescence experiments required the use of different DOX concentrations, and the DOX monomer−dimer equilibrium was not included in the analysis.

Chemical Stability of the Bound DOX. After storage of the MOF-DOX suspensions for 24 h in the dark at 22 °C, the UV−vis absorption (and the CD spectra) remained qualitatively similar to those of the freshly prepared samples. (See Figure 5.) Some precipitation was observed, especially for MOF contents >0.1 mg/mL, and a slight decrease in the DOX alone sample signal was likely due to drug sticking on the glass test tube. These effects can account for the shift of the two

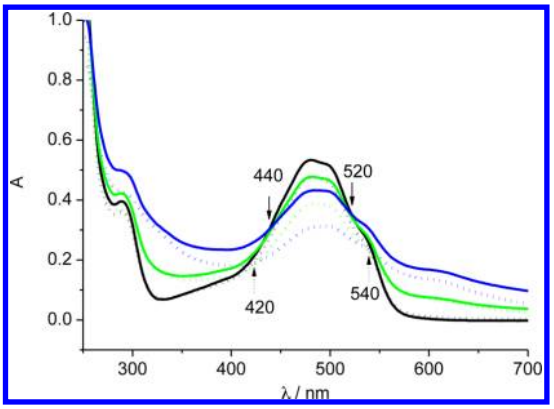

Figure 5. UV−vis absorption spectra DOX 1×10^{-4} M in neutral Tris buffer 10 mM pH 7.4, alone (black) and in the presence of MIL-100 (Fe) 0.1 mg/mL (green) and 0.3 mg/mL (blue), freshly prepared samples (solid lines), and samples stored in the dark at 22 °C after 24 h (dotted lines). Cell path length 0.5 cm; references for the mixtures are the relevant empty MOF samples.

isosbestic points from 440 and 520 nm to 420 and 540 nm, respectively.

These results are in agreement with previous observations about stability of DOX released from the MOFs over several days[24] and differ from literature reporting degradation of DOX complexed to Fe(III) salts in aqueous solution.[49−52] Indeed, under experimental conditions similar to those of the present study, DOX self-reduction with a rate constant of 0.076 min^{-1} has been observed and assigned to the formation of a Fe(II)-DOX^+ species upon Fe(III) coordination at the DOX α-ketol group. It has been suggested that such reaction mediates mutagenic and cytotoxic effects in living cells through Fe-based free-radical-induced oxidative stress. Other studies have reported about Fe(III) complexes bearing three DOX molecules that undergo chemical modification of one drug molecule out of three,[63] although the importance of such reactions under pharmacological conditions has been questioned.[48] The remarkable stability of DOX within the MOF frame over many hours points to an effective inhibition of free-radical chemistry in the system.

CONCLUSIONS

In this study, we have shown that DOX, known to be incorporated into MIL-100 (Fe) nanoparticles up to 9 wt %,[24] binds upon the formation of highly stable coordination bonds to CUS of Fe(III) centers and disruption of drug self-associated species. On the basis of the UV−vis absorption and CD spectral features of DOX-MOF mixtures, we have concluded that DOX coordination occurs to one or two negatively charged oxygen centers of the B ring, upon deprotonation of the relevant hydroxyl groups. (See Schemes 1 and 3.) The absence of fluorescence from the DOX complexes is consistent with such a mechanism. DLS showed that at MOF contents >0.2 mg/mL, nanoparticle aggregation occurs both in Tris buffer and in water, likely due to DOX bridging of external Fe(III) centers of different particles to form a DOX-MOF cross-linked coordination network. In water, in freshly prepared samples, the DOX-loaded nanoparticle average size is <250 nm with MOF contents <0.2 mg/mL.

Complexed DOX neither undergoes degradation under aerobic conditions nor exhibits any lability under visible-light excitation, thereby showing that the MIL-100 (Fe) matrix

dx.doi.org/10.1021/jp503809w | J. Phys. Chem. B 2014, 118, 8532−8539

effectively inhibits iron-mediated, thermal, or photoinduced free radical chemistry.

■ ASSOCIATED CONTENT

Supporting Information

X ray powder diffraction patterns of MIL-100(Fe) and electron microscopy of relevant nanoMOF samples in both absence and presence of DOX. Dynamic light scattering of MIL-100(Fe) nanoMOFs in water in both absence and presence of DOX. Fluorescence decay of DOX in the presence of MIL-100(Fe) nanoMOFs in Tris buffer. This material is available free of charge via the Internet at http://pubs.acs.org.

■ AUTHOR INFORMATION

Notes

The authors declare no competing financial interest.

■ ACKNOWLEDGMENTS

Funding of the research was from the FP7 PEOPLE-ITN project no. 237962-CYCLON. We thank Dr. Andrea Zattoni and Dr. Barbara Roda (Dipartimento di Chimica "G. Ciamician", Università di Bologna) for helpful discussions and byFlow Srl (Bologna, Italy) for supporting light scattering facilities. We also thank Dr. Anna Costa (CNR, Istituto di Scienza e Tecnologia dei Materiali Ceramici) for SEM measurements.

■ REFERENCES

(1) Couvreur, P.; Gref, R.; Andrieux, K.; Malvy, C. Nanotechnologies for Drug Delivery: Application to Cancer and Autoimmune Diseases. *Prog. Solid State Chem.* **2006**, *34*, 231−235.

(2) Peer, D.; Karp, J. M.; Hong, S.; FaroKhzad, O. C.; Margalit, R.; Langer, R. Nanocarriers as an Emerging Platform for Cancer Therapy. *Nat. Nanotechnol.* **2007**, *2*, 751−760.

(3) Riehemann, K.; Schneider, S. W.; Luger, T. A.; Godin, B.; Ferrari, M.; Fuchs, H. Nanomedicine-Challenge and Perspectives. *Angew. Chem., Int. Ed.* **2009**, *48*, 872−897.

(4) Wang, M.; Thanou, M. Targeting Nanoparticles to Cancer. *Pharmacol. Res.* **2010**, *62*, 90−99.

(5) Cho, K.; Wang, X.; Nie, S.; Chen, Z.; Shin, D. M. Therapeutic Nanoparticles for Drug Delivery in Cancer. *Clin. Cancer Rev.* **2008**, *14*, 1310−1316.

(6) Gabizon, A. A. Pegylated Liposomal Doxorubicin: Metamorphosis of an Old Drug into a New Form of Chemotherapy. *Cancer Invest.* **2001**, *19*, 424−436.

(7) Gabizon, A.; Shmeeda, H.; Barenholz, Y. Pharmacokinetics of Pegylated Liposomal Doxorubicin - Review of Animal and Human Studies. *Clin. Pharmacokinet.* **2003**, *42*, 419−436.

(8) Batist, G.; Harris, L.; Azarnia, N.; Lee, L. W.; Daza-Ramirez, P. Improved Anti-Tumor Response Rate with Decreased Cardiotoxicity of Non-Pegylated Liposomal Doxorubicin Compared with Conventional Doxorubicin in First-Line Treatment of Metastatic Breast Cancer in Patients Who Had Received Prior Adjuvant Doxorubicin: Results of a Retrospective Analysis. *Anti-Cancer Drugs* **2006**, *17*, 587−595.

(9) Miele, E.; Spinelli, G. P.; Miele, E.; Tomao, F.; Tomao, S. Albumin-Bound Formulation of Paclitaxel (Abraxane (R) ABI-007) in the Treatment of Breast Cancer. *Int. J. Nanomed.* **2009**, *4*, 99−105.

(10) Torchilin, V. P. Multifunctional Nanocarriers. *Adv. Drug Delivery Rev.* **2006**, *58*, 1532−1555.

(11) Li, H.; Eddaoudi, M.; O'Keeffe, M.; Yaghi, O. M. Design and Synthesis of an Exceptionally Stable and Highly Porous Metal-Organic Framework. *Nature* **1999**, *402*, 276−279.

(12) Meek, S. T.; Greathouse, J. A.; Allendorf, M. D. Metal-Organic Frameworks: A Rapidly Growing Class of Versatile Nanoporous Materials. *Adv. Mater.* **2011**, *23*, 249−267.

(13) Sanchez, C.; Julian, B.; Belleville, P.; Popall, M. Applications of Hybrid Organic-Inorganic Nanocomposites. *J. Mater. Chem.* **2005**, *15*, 3559−3592.

(14) Lee, J.; Farha, O. K.; Roberts, J.; Scheidt, K. A.; Nguyen, S. T.; Hupp, J. T. Metal-Organic Framework Materials as Catalysts. *Chem. Soc. Rev.* **2009**, *38*, 1450−1459.

(15) Allendorf, M. D.; Bauer, C. A.; Bhakta, R. K.; Houk, R. J. T. Luminescent Metal-Organic Frameworks. *Chem. Soc. Rev.* **2009**, *38*, 1330−1352.

(16) Hinks, N. J.; McKinlay, A. C.; Xiao, B.; Wheatley, P. S.; Morris, R. E. Metal Organic Frameworks as NO Delivery Materials for Biological Applications. *Microporous Mesoporous Mater.* **2008**, *129*, 330−334.

(17) McKinlay, A. C.; Morris, R. E.; Horcajada, P.; Ferey, G.; Gref, R.; Couvreur, P.; Serre, C. Biomofs: Metal-Organic Frameworks for Biological and Medical Applications. *Angew. Chem., Int. Ed.* **2010**, *49*, 6260−6266.

(18) Miller, S. R.; Heurtaux, D.; Baati, T.; Horcajada, P.; Greneche, J.-M.; Serre, C. Biodegradable Therapeutic MOFs for the Delivery of Bioactive Molecules. *Chem. Commun.* **2010**, *46*, 4526−4528.

(19) Chen, B.; Xiang, S.; Qian, G. Metal-Organic Frameworks with Functional Pores for Recognition of Small Molecules. *Acc. Chem. Res.* **2010**, *43*, 1115−1124.

(20) Huxford, R. C.; Della Rocca, J.; Lin, W. Metal-Organic Frameworks as Potential Drug Carriers. *Curr. Opin. Chem. Biol.* **2010**, *14*, 262−268.

(21) Horcajada, P.; Gref, R.; Baati, T.; Allan, P. K.; Maurin, G.; Couvreur, P.; Ferey, G.; Morris, R. E.; Serre, C. Metal-Organic Frameworks in Biomedicine. *Chem. Rev.* **2012**, *112*, 1232−1268.

(22) Zhou, H. C.; Long, J. R.; Yaghi, O. M. Introduction to Metal-Organic Frameworks. *Chem. Rev.* **2012**, *112*, 673−674.

(23) Chalati, T.; Horcajada, P.; Couvreur, P.; Serre, C.; Ben Yahia, M.; Maurin, G.; Gref, R. Porous Metal Organic Framework Nanoparticles to Address the Challenges Related to Busulfan Encapsulation. *Nanomedicine* **2011**, *6*, 1683−1695.

(24) Horcajada, P.; Chalati, T.; Serre, C.; Gillet, B.; Sebrie, C.; Baati, T.; Eubank, J. F.; Heurtaux, D.; Clayette, P.; Kreuz, C.; et al. Porous Metal-Organic-Framework Nanoscale Carriers as a Potential Platform for Drug Delivery and Imaging. *Nat. Mater.* **2010**, *9*, 172−178.

(25) Horcajada, P.; Serre, C.; Vallet-Regi, M.; Sebban, M.; Taulelle, F.; Ferey, G. Metal-Organic Frameworks as Efficient Materials for Drug Delivery. *Angew. Chem., Int. Ed.* **2006**, *45*, 5974−5978.

(26) Horcajada, P.; Surble, S.; Serre, C.; Hong, D.-Y.; Seo, Y.-K.; Chang, J.-S.; Greneche, J.-M.; Margiolaki, I.; Ferey, G. Synthesis and Catalytic Properties of MIL-100(Fe), an Iron(III) Carboxylate with Large Pores. *Chem. Commun.* **2007**, 2820−2822.

(27) Agostoni, V.; Anand, R.; Monti, S.; Hall, S.; Maurin, G.; Horcajada, P.; Serre, C.; Bouchemal, K.; Gref, R. Impact of Phosphorylation on the Encapsulation of Nucleoside Analogues within Porous Iron(III) Metal-Organic Framework MIL-100(Fe) Nanoparticles. *J. Mater. Chem. B* **2013**, *1*, 4231−4242.

(28) Marquez, A. G.; Demessence, A.; Platero-Prats, A. E.; Heurtaux, D.; Horcajada, P.; Serre, C.; Chang, J.-S.; Ferey, G.; Antonio de la Pena-O'Shea, V.; Boissiere, C.; et al. Green Microwave Synthesis of MIL-100(Al, Cr, Fe) Nanoparticles for Thin-Film Elaboration. *Eur. J. Inorg. Chem.* **2012**, 5165−5174.

(29) Seo, Y.-K.; Yoon, J. W.; Lee, J. S.; Lee, U. H.; Hwang, Y. K.; Jun, C.-H.; Horcajada, P.; Serre, C.; Chang, J.-S. Large Scale Fluorine-Free Synthesis of Hierarchically Porous Iron(III) Trimesate MIL-100(Fe) with a Zeolite Mtn Topology. *Microporous Mesoporous Mater.* **2012**, *157*, 137−145.

(30) Beretta, G. L.; Zunino, F. Molecular Mechanisms of Anthracycline Activity. In *Anthracycline Chemistry and Biology II: Mode of Action, Clinical Aspects and New Drugs*; Springer-Verlag: Berlin; Vol. *283*, pp 1−19.

(31) Minotti, G.; Menna, P.; Salvatorelli, E.; Cairo, G.; Gianni, L. Anthracyclines: Molecular Advances and Pharmacologic Developments in Antitumor Activity and Cardiotoxicity. *Pharmacol. Rev.* **2004**, *56*, 185−229.

(32) Beraldo, H.; Garnier-Suillerot, A.; Tosi, L.; Lavelle, F. Iron(III) Adriamycin and Iron(III) Daunorubicin Complexes - Physicochemical Characteristics, Interaction with DNA, and Antitumor-Activity. *Biochemistry* **1985**, *24*, 284−289.
(33) Dalmark, M.; Storm, H. H. A Fickian Diffusion Transport Process with Features of Transport Catalysis-Doxorubicin Transport in Human Red-Blood-Cells. *J. Gen. Physiol.* **1981**, *78*, 349−364.
(34) Nakanishi, T.; Fukushima, S.; Okamoto, K.; Suzuki, M.; Matsumura, Y.; Yokoyama, M.; Okano, T.; Sakurai, Y.; Kataoka, K. Development of the Polymer Micelle Carrier System for Doxorubicin. *J. Controlled Release* **2001**, *74*, 295−302.
(35) Krishna, R.; Mayer, L. D. Multidrug Resistance (MDR) in Cancer - Mechanisms, Reversal Using Modulators of MDR and the Role of MDR Modulators in Influencing the Pharmacokinetics of Anticancer Drugs. *Eur. J. Pharm. Sci.* **2000**, *11*, 265−283.
(36) Cerroni, B.; Chiessi, E.; Margheritelli, S.; Oddo, L.; Paradossi, G. Polymer Shelled Microparticles for a Targeted Doxorubicin Delivery in Cancer Therapy. *Biomacromolecules* **2011**, *12*, 593−601.
(37) Huang, H.; Yuan, Q.; Shah, J. S.; Misra, R. D. K. A New Family of Folate-Decorated and Carbon Nanotube-Mediated Drug Delivery System: Synthesis and Drug Delivery Response. *Adv. Drug Delivery Rev.* **2011**, *63*, 1332−1339.
(38) Lowery, A.; Onishko, H.; Hallahan, D. E.; Han, Z. Z. Tumor-Targeted Delivery of Liposome-Encapsulated Doxorubicin by Use of a Peptide that Selectively Binds to Irradiated Tumors. *J. Controlled Release* **2011**, *150*, 117−124.
(39) Huynh, C. T.; Nguyen, M. K.; Kim, J. H.; Kang, S. W.; Kim, B. S.; Lee, D. S. Sustained Delivery of Doxorubicin Using Biodegradable pH/Temperature-Sensitive Poly(Ethylene Glycol)-Poly(β-Amino Ester Urethane) Multiblock Copolymer Hydrogels. *Soft Matter* **2011**, *7*, 4974−4982.
(40) Anand, R.; Manoli, F.; Manet, I.; Daoud-Mahammed, S.; Agostoni, V.; Gref, R.; Monti, S. β-Cyclodextrin Polymer Nanoparticles as Carriers for Doxorubicin and Artemisinin: A Spectroscopic and Photophysical Study. *Photochem. Photobiol. Sci.* **2012**, *11*, 1285−1292.
(41) Yoon, J. W.; Seo, Y.-K.; Hwang, Y. K.; Chang, J.-S.; Leclerc, H.; Wuttke, S.; Bazin, P.; Vimont, A.; Daturi, M.; Bloch, E.; et al. Controlled Reducibility of a Metal-Organic Framework with Coordinatively Unsaturated Sites for Preferential Gas Sorption. *Angew. Chem., Int. Ed.* **2010**, *49*, 5949−5952.
(42) Anand, R.; Ottani, S.; Manoli, F.; Manet, I.; Monti, S. A Close-up on Doxorubicin Binding to γ-Cyclodextrin: An Elucidating Spectroscopic, Photophysical and Conformational Study. *RSC Adv.* **2012**, *2*, 2346−2357.
(43) Glebov, E. M.; Pozdnyakov, I. P.; Grivin, V. P.; Plyusnin, V. F.; Zhang, X.; Wu, F.; Deng, N. Intermediates in Photochemistry of Fe(III) Complexes with Carboxylic Acids in Aqueous Solutions. *Photochem. Photobiol. Sci.* **2011**, *10*, 425−430.
(44) Fiallo, M. M. L.; Tayeb, H.; Suarato, A.; Garnier-Suillerot, A. Circular Dichroism Studies on Anthracycline Antitumor Compounds. Relationship between the Molecular Structure and the Spectroscopic Data. *J. Pharm. Sci.* **1998**, *87*, 967−975.
(45) Gallois, L.; Fiallo, M.; Garnier-Suillerot, A. Comparison of the Interaction of Doxorubicin, Daunorubicin, Idarubicin and Idarubicinol with Large Unilamellar Vesicles - Circular Dichroism Study. *Biochim. Biophys. Acta, Biomembr.* **1998**, *1370*, 31−40.
(46) Sturgeon, R. J.; Schulman, S. G. Electronic Absorption-Spectra and Protolytic Equilibria of Doxorubicin - Direct Spectrophotometric Determination of Microconstants. *J. Pharm. Sci.* **1977**, *66*, 958−961.
(47) Fiallo, M. M. L.; Drechsel, H.; Garnier-Suillerot, A.; Matzanke, B. F.; Kozlowski, H. Solution Structure of Iron(III)-Anthracycline Complexes. *J. Med. Chem.* **1999**, *42*, 2844−2851.
(48) Fiallo, M. M. L.; Garnier-Suillerot, A.; Matzanke, B.; Kozlowski, H. How Fe^{3+} Binds Anthracycline Antitumour Compounds - the Myth and the Reality of a Chemical Sphinx. *J. Inorg. Biochem.* **1999**, *75*, 105−115.
(49) Hasinoff, B. B. Self-Reduction of the Iron(III)-Doxorubicin Complex. *Free Radic. Biol. Med.* **1989**, *7*, 583−593.
(50) Malisza, K. L.; Hasinoff, B. B. Production of Hydroxyl Radical by Iron(III)-Anthraquinone Complexes through Self-Reduction and through Reductive Activation by the Xanthine-Oxidase Hypoxanthine System. *Arch. Biochem. Biophys.* **1995**, *321*, 51−60.
(51) Malisza, K. L.; Hasinoff, B. B. Doxorubicin Reduces the Iron(III) Complexes of the Hydrolysis Products of the Antioxidant Cardioprotective Agent Dexrazoxane (ICRF-187) and Produces Hydroxyl Radicals. *Arch. Biochem. Biophys.* **1995**, *316*, 680−688.
(52) Eizaguirre, A.; Yanez, M.; Eriksson, L. A. Stability and Iron Coordination in DNA Adducts of Anthracycline Based Anti-Cancer Drugs. *Phys. Chem. Chem. Phys.* **2012**, *14*, 12505−12514.
(53) Nawara, K.; McCracken, J. L.; Krysinski, P.; Blanchard, G. J. Structure-Dependent Complexation of Fe^{3+} by Anthracyclines. 1. The Importance of Pendent Hydroxyl Functionality. *J. Phys. Chem. B* **2013**, *117*, 6859−6867.
(54) Gianni, L.; Vigano, L.; Lanzi, C.; Niggeler, M.; Malatesta, V. Role of Daunosamine and Hydroxyacetyl Side-Chain in Reaction with Iron and Lipid-Peroxidation by Anthracyclines. *J. Natl. Cancer Inst.* **1988**, *80*, 1104−1111.
(55) Nawara, K.; Beeckman, H.; Krysinski, P.; Blanchard, G. J. Structure-Dependent Complexation of Fe^{3+} by Anthracyclines. 2. The Roles of Methoxy and Daunosamine Functionalities. *J. Phys. Chem. B* **2013**, *117*, 6868−6873.
(56) Lin, W.; Rieter, W. J.; Taylor, K. M. L. Modular Synthesis of Functional Nanoscale Coordination Polymers. *Angew. Chem., Int. Ed.* **2009**, *48*, 650−658.
(57) Spokoyny, A. M.; Kim, D.; Sumrein, A.; Mirkin, C. A. Infinite Coordination Polymer Nano- and Microparticle Structures. *Chem. Soc. Rev.* **2009**, *38*, 1218−1227.
(58) Zhu, M.; Nie, G.; Meng, H.; Xia, T.; Nel, A.; Zhao, Y. Physicochemical Properties Determine Nanomaterial Cellular Uptake, Transport, and Fate. *Acc. Chem. Res.* **2013**, *46*, 622−631.
(59) Agostoni, V.; Chalati, T.; Horcajada, P.; Willaime, H.; Anand, R.; Semiramoth, N.; Baati, T.; Hall, S.; Maurin, G.; Chacun, H.; et al. Towards an Improved Anti-Hiv Activity of NRTI Via Metal−Organic Frameworks Nanoparticles. *Adv. Healthcare Mater.* **2013**, *2*, 1630−1637.
(60) Agostoni, V.; Horcajada, P.; Rodriguez-Ruiz, V.; Willaime, H.; Couvreur, P.; Serre, C.; Gref, R. 'Green' Fluorine-Free Mesoporous Iron(III) Trimesate Nanoparticles for Drug Delivery. *Green Mater.* **2013**, *1*, 209−217.
(61) Changenet-Barret, P.; Gustavsson, T.; Markovitsi, D.; Manet, I.; Monti, S. Unravelling Molecular Mechanisms in the Fluorescence Spectra of Doxorubicin in Aqueous Solution by Femtosecond Fluorescence Spectroscopy. *Phys. Chem. Chem. Phys.* **2013**, *15*, 2937−2944.
(62) Lakowicz, J. R. *Principles of Fluorescence Spectroscopy*, 3rd ed.; Springer: New York, 2006.
(63) Fiallo, M.; Laigle, A.; Borrel, M. N.; Garnier-Suillerot, A. Accumulation of Degradation Products of Doxorubicin and Pirarubicin Formed in Cell Culture Medium within Sensitive and Resistant Cells. *Biochemistry* **1993**, *45*, 659−665.